IEEE Access
Multidisciplinary ⋮ Rapid Review ⋮ Open Access Journal

Received January 2, 2017, accepted January 19, 2017, date of publication January 27, 2017, date of current version March 13, 2017.

Digital Object Identifier 10.1109/ACCESS.2017.2660302

A Region-Wised Medium Transmission Based Image Dehazing Method

HUI YUAN[1], (Member, IEEE), CHANGCHUN LIU[1, 2], ZHIXIN GUO[1], AND ZHENZHEN SUN[1]

Received January 2, 2017, accepted January 19, 2017.Date of publication xxxx 00, 0000, date of current version xxxx 00, 0000.

[1]School of Information Science and Engineering, Shandong University, Jinan 250100, China
[2]Troops 61541, Chinese People's Liberation Army, Beijing 100094, China

Corresponding author: H. Yuan (yuanhui0325@gmail.com)

This work was supported in part by the National Natural Science Foundation of China under Grant 61571274, in part by the Shandong Natural Science Funds for Distinguished Young Scholar under Grant JQ201614, and in part by the Young Scholars Program of Shandong University under Grant 2015WLJH39.

ABSTRACT Image dehazing is a technique to enhance the images acquired in poor weather conditions, such as fog and haze. Existing image dehazing methods are mainly based on dark channel prior. Since the dark channel is not reasonable for sky regions, a sky segmentation and region wised medium transmission based image dehazing method is proposed in this paper. Firstly, sky regions are segmented by quad-tree splitting based feature pixels detection. Then, a medium transmission estimation method for sky regions is proposed based on color characteristic observation of sky regions. The medium transmission is then filtered by an edge preserving guided filter. Finally, based on the estimated medium transmission, the hazed images are restored. Experimental results demonstrate that the performance of the proposed method is better than that of existing methods. The restored image is more natural, especially in the sky regions.

INDEX TERMS Image dehazing, image segmentation, dark channel prior.

I. INTRODUCTION

Outdoor scenes usually suffer from suspended atmospheric particles such as mill dust, vapor, smoke, etc. which reduce the quality of the images greatly. The visibility, contrast and vividness of the scene can be drastically degraded by the suspended atmospheric particles, as shown in Fig. 1 [1]. Thus, it is difficult to distinguish objects in the scene. Image dehazing is a technique to enhance the images acquired in poor weather conditions, *e.g.* fog and haze. It has become a critical problem in applications such as aerial imaging, driver assistance, and visual surveillance [2] *etc*. The goal of image dehazing is to restore the visibility of the scene.

In recent years, lots of image dehazing algorithms have been proposed, as reviewed in [3]. There are mainly three kinds of image dehazing method, *i.e.* contrast enhancement based image dehazing method [4], special image capture equipment based dehazing method [5], and atmospheric physical model based image dehazing method [6], [7], etc. *Tan* [4] assumes that the contrast of a haze-free image is higher than that of the hazed image. Based on the assumption, the image dehazing algorithm in [4] was designed by maximizing the image contrast of local areas with constant environment light. Although the image visibility is improved significantly, there are usually halo artifacts [8] and over-stretches contrast in dehazed images. In [5], a polarization method is proposed to remove haze by investigating the polarization characteristics form two images obtained by rotating a polarizing filter to different angles. Although the performance of this method is good, it needs a special hardware configuration that attaches the polarization filter to the camera. *He et al.* [6] proposed a dehazing algorithm based

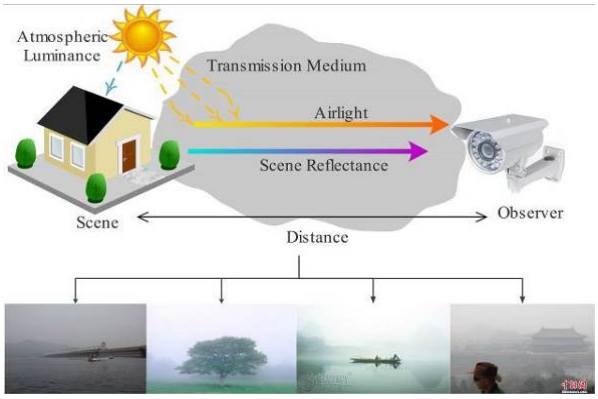

FIGURE 1. Images with fog or haze [1], from left to right: ***wharf***, ***tree***, ***boat***, and ***man_in_haze***.

on the dark channel prior. The dark channel prior means that there are at least one color channel with pixel values close to zero in the haze-free image. Based on the dark channel prior, the medium transmission can be roughly estimated. Then, the final dehazed image is generated from the medium transmission which is refined by soft matting [9] or guided filter [10]. The dehazed image of *He's* method is more close to the real scene even if there is a dense fog. However, since the dark channel prior is only suitable for non-sky regions, the performance of *He's* method is not perfect in sky regions. To address the problem, an image dehazing method was proposed based on sky region segmentation in [7]. In this method, sky regions were first detected through brightness and gradient. Then, the medium transmissions of sky regions and non-sky regions are estimated respectively so as to restore the hazed image. Because that the segmentation effect is not satisfactory, and the estimated medium transmission of sky regions is not accurate enough, the performance of this method is also not perfect, especially when the scene suffers dense fog.

In order to further improve the quality of dehazed images, quad-tree splitting [11] based feature pixels detection for sky region segmentation is proposed first. Then, based on the color characteristic observation of sky regions, a medium transmission estimation method for sky regions is proposed. After that, the medium transmission is filtered by an edge preserving guided filter. Based on the estimated medium transmission, the hazed images can be restored perfectly, especially in sky regions. The reminder of this paper is organized as follows. In section II, background theory of image dehazing is introduced briefly. The proposed method is presented in Section III in detail. Experimental results and conclusions are given in Section IV and V respectively.

II. BACKGROUND THEORY

A. ATMOSPHERIC SCATTERING MODEL

A hazy image is generated from a haze-free image by the following atmospheric scattering model [12],

$$\mathbf{I}(\mathbf{x}) = \mathbf{J}(\mathbf{x}) .^{*}\mathbf{t}(\mathbf{x}) + \mathbf{A}.^{*}[\mathbf{1} - \mathbf{t}(\mathbf{x})], \tag{1}$$

where $\mathbf{x}$ is pixel position, $\mathbf{I}$ is the observed intensity, i.e., the hazy image, $\mathbf{J}$ is the scene radiance, i.e., the haze-free image, $\mathbf{A}$ is the global atmospheric light, $\mathbf{t}$ is the medium transmission describing the portion of the light that can reach the camera, and $.^{*}$ represents the corresponding points multiplication. In the right hand of (1), the term $\mathbf{J}(\mathbf{x}) .^{*}\mathbf{t}(\mathbf{x})$ is called as *direct attenuation* [6] which describes the scene radiance and its decay in the medium, while the other term $\mathbf{A}.^{*}[\mathbf{1} - \mathbf{t}(\mathbf{x})]$ denotes the *airlight* [6], [12], resulting from previously scattered light and leads to the shift of the scene colors. The aim of image dehazing is to restore the haze-free image $\mathbf{J}$ from the observed hazy image $\mathbf{I}$. Therefore, the global atmospheric light $\mathbf{A}$, the medium transmission $\mathbf{t}$ must be estimated.

B. DARK CHANNEL PRIOR BASED IMAGE DEHAZING

The dark channel prior describes a fact that in most of the non-sky patches of outdoor haze-free images, there are at least one color channel which have near zero pixel intensities [6]. For a haze-free image $\mathbf{J}$, the dark channel $\mathbf{J}^{\mathbf{dark}}$ can be represented as,

$$\mathbf{J}^{\mathbf{dark}}(\mathbf{x}) = \min_{\mathbf{y}\in\boldsymbol{\Omega}(\mathbf{x})}\left[\min_{c\in\{r,g,b\}}\mathbf{J}^{c}(\mathbf{y})\right], \tag{2}$$

where $\mathbf{J}^{\mathbf{c}}$ represents the color channel, $\boldsymbol{\Omega}(\mathbf{x})$ denotes a local patch centered at position $\mathbf{x}$. Accordingly, based on the dark channel prior, $\mathbf{J}^{\mathbf{dark}}(\mathbf{x})$ for non-sky patches tends to be zero,

$$\mathbf{J}^{\mathbf{dark}}(\mathbf{x}) \to \mathbf{0}. \tag{3}$$

Thus, if the global atmospheric light $\mathbf{A}$ is given, (4) can be derived,

$$\mathbf{I}^{c}(\mathbf{x})./\mathbf{A}^{c} = \left[\mathbf{t}(\mathbf{x}) .^{*} \mathbf{J}^{c}(\mathbf{x})\right]./\mathbf{A}^{c} + \mathbf{1} - \mathbf{t}(\mathbf{x}), \tag{4}$$

where the subscript $c \in \{r, g, b\}$ denotes color channels, $./$ represents dividing operation between corresponding points. Assuming that the medium transmission $\mathbf{t}(\mathbf{x})$ in a local patch $\boldsymbol{\Omega}(\mathbf{x})$ is constant which can be rewritten as $\tilde{\mathbf{t}}(\mathbf{x})$, (4) can be further derived as (5) by taking two consecutive minimum operators on both sides,

$$\begin{aligned}&\min_{\mathbf{y}\in\boldsymbol{\Omega}(\mathbf{x})}\left(\min_{c\in\{r,g,b\}}\left(\mathbf{I}^{c}(\mathbf{y})./\mathbf{A}^{c}\right)\right)\\ &\quad= \tilde{\mathbf{t}}(\mathbf{x}).^{*}\min_{\mathbf{y}\in\boldsymbol{\Omega}(\mathbf{x})}\left(\min_{c\in\{r,g,b\}}\left(\mathbf{J}^{c}(\mathbf{y})./\mathbf{A}^{c}\right)\right) + \mathbf{1} - \tilde{\mathbf{t}}(\mathbf{x}),\end{aligned} \tag{5}$$

where $\min_{\mathbf{y}\in\boldsymbol{\Omega}(\mathbf{x})}(\min_{c\in\{r,g,b\}}\mathbf{I}^{c}(\mathbf{y}))$ can be thought as the dark channel of the input hazed image. By taking (2) and (3) into (5), $\tilde{\mathbf{t}}(\mathbf{x})$ can be written as,

$$\tilde{\mathbf{t}}(\mathbf{x}) = \mathbf{1} - \min_{\mathbf{y}\in\boldsymbol{\Omega}(\mathbf{x})}\left(\min_{c\in\{r,g,b\}}\left(\mathbf{I}^{c}(\mathbf{y})./\mathbf{A}^{c}\right)\right). \tag{6}$$

As a result, the medium transmission can be estimated directly from the hazy image. To make the image natural and retain a good feeling of depth [6], (6) is modified by a constant coefficient $\omega(0 < \omega < 1)$ which is set as 0.95 empirically,

$$\tilde{\mathbf{t}}(\mathbf{x}) = \mathbf{1} - \omega\cdot\min_{\mathbf{y}\in\boldsymbol{\Omega}(\mathbf{x})}\left(\min_{c\in\{r,g,b\}}\left(\mathbf{I}^{c}(\mathbf{y})./\mathbf{A}^{c}\right)\right). \tag{7}$$

Furthermore, in order to remove the halos and block artifacts of the medium transmission matrix (or named as transmission image), soft matting [9], guide filter [10], or bilateral filter [13], or can also be used to modify $\tilde{\mathbf{t}}(\mathbf{x})$.

Besides, since in the most dense haze region, i.e., the light of the brightest regions in dark channel is only determined by global atmospheric light$\mathbf{A}$ [6], the global atmospheric light $\mathbf{A}$ can be estimated from the dark channel $\mathbf{J}^{\mathbf{dark}}$ directly. The 10% brightest pixels of the dark channel is first picked up. Then among these selected pixels, the pixels with highest intensity in the input hazy image $\mathbf{I}$ are chosen as the global atmospheric light.

As a result, once the medium transmission $\tilde{\mathbf{t}}(\mathbf{x})$ and the global atmospheric light $\mathbf{A}$ are estimated, the haze-free image can be restored by (8),

$$\begin{aligned}\mathbf{J}(\mathbf{x}) &= \left\{\mathbf{I}(\mathbf{x}) - \mathbf{A}.^{*}\left[\mathbf{1} - \tilde{\mathbf{t}}(\mathbf{x})\right]\right\}./\tilde{\mathbf{t}}(\mathbf{x}) \\ &= \left\{\mathbf{I}(\mathbf{x}) - \mathbf{A} + \mathbf{A}.^{*}\tilde{\mathbf{t}}(\mathbf{x})\right\}./\tilde{\mathbf{t}}(\mathbf{x}) \\ &= \{\mathbf{I}(\mathbf{x}) - \mathbf{A}\}./\tilde{\mathbf{t}}(\mathbf{x}) + \mathbf{A}. \end{aligned} \tag{8}$$

In order to restrict $\mathbf{J}(\mathbf{x})$ to be a limited value, (8) is further modified as,

$$\mathbf{J}(\mathbf{x}) = \{\mathbf{I}(\mathbf{x}) - \mathbf{A}\}./\left\{\mathbf{max}\left[\tilde{\mathbf{t}}(\mathbf{x}), t_0\right]\right\} + \mathbf{A}, \tag{9}$$

where t_0 is set as 0.1 empirically.

The performance of dark channel prior based image dehazing method is well, however, there still exists unnatural halos in sky regions because of the inherent drawback of dark channel prior. Therefore, sky regions are first segmented from a hazed image, and then treat the sky and non-sky regions distinctively so as to improve restored image quality.

III. PROPOSED METHOD

The dark channel prior is observed from patches in non-sky regions. Therefore, there is an inherent defect that the quality of a dehazed image is unsatisfactory in sky region [6]. In the proposed method, sky region is first segmented form the input hazy image. Then, an adaptive patch size based Dark Channel Prior for hazy image are proposed. After that, a region-wised medium transmission are calculated separately based on Color Characteristics of Sky Region (CCSR) and Dark Channel Prior for non-Sky Region (DCPnSR). Finally, a low complexity edge preserving guided filter is proposed to smooth the medium transmission so as to restore the input hazy image.

FIGURE 2. Segmentation results by mean shift algorithm, different regions are distinguished by different grey values, from left to right: *wharf*, *tree*, *boat*, and *man_in_haze*.

A. MEAN SHIFT BASED SKY REGION SEGMENTATION

The input image is first segmented into lots of areas, denoted as $\mathbf{S} = \{s_1, s_2, \ldots, s_\Theta\}$, based on the luminance of each pixel by mean shift algorithm [14]. Detailed segmentation results are shown in Fig. 2.

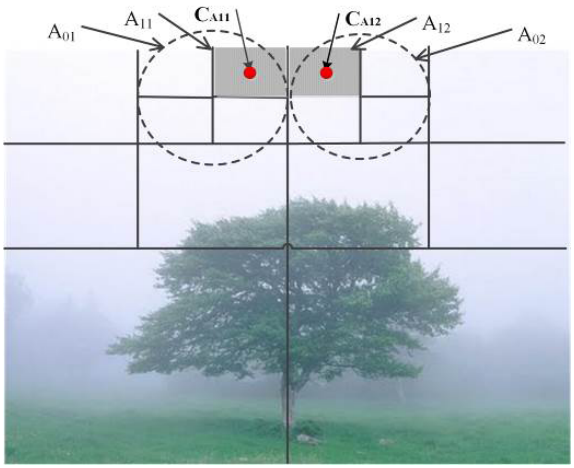

FIGURE 3. Quadtree based feature pixels searching for sky region segmentation.

Furthermore, based on the observation that a sky region is usually smooth, with high brightness, located on the top of an image, and maybe separated by high buildings or trees, etc., a quadtree based feature pixels searching method is proposed so as to extract sky regions from $\mathbf{S}$. Firstly, the input image is evenly divided into four regions, as shown in Fig. 3. Due to that sky region is usually located on the top of an image, the top left and the top right blocks are further divided into four sub-blocks, denoted as, $\Delta_{\text{left},1}$, $\Delta_{\text{left},2}$, $\Delta_{\text{left},3}$, $\Delta_{\text{left},4}$, $\Delta_{\text{right},1}$, $\Delta_{\text{right},2}$, $\Delta_{\text{right},3}$, and, $\Delta_{\text{right},4}$ respectively, as shown in Fig. 3. Secondly, the average brightness and average gradient of each sub-block are calculated by (10) and (11),

$$I_{\varphi,i}^{light} = \frac{1}{N_{left,i}} \sum_{n=1}^{N_{left,1}} \left(\frac{1}{3} \sum_{c\in\{r,g,b\}} I^c(n) \right), \tag{10}$$

$$I_{\varphi,i}^{grad} = \frac{1}{N_{\varphi,i}} \sum_{n\in\Delta_{\varphi,i}} \left(\frac{1}{3} \sum_{c\in\{r,g,b\}} \frac{\partial(I^c(n))}{\partial n} \right), \tag{11}$$

where $\varphi \in \{left, right\}$, $N_{left,i}$ is the number of pixels in the sub-block $\Delta_{\varphi,i}$, $I^c(n)$ refers to the pixel of n^{th} pixel in the color component c, and $c \in \{r, g, b\}$. Subsequently, two sub-blocks (one corresponds to $\varphi = left$, and is denoted as A_{01}; while the other corresponds to $\varphi = right$, and is denoted as A_{02}) are selected by solving (12),

$$\arg\max_{i} \left\{ I_{\varphi,i}^{light} \right\}, \tag{12}$$

where

$$i \in \left\{ 0, 1, 2, 3, |I_{\varphi,i}^{grad} \le \frac{1}{4} \sum_{i=1}^{4} I_{\varphi,i}^{grad} \right\}. \tag{13}$$

The two sub-blocks A_{01} and A_{02} are then further split into 4 micro-blocks respectively. By repeating calculation of (10)-(13), the two micro-blocks A_{11} and A_{12} can be selected, as shown in Fig. 3. Thirdly, the two center pixels C_{A11} and C_{A12} of the two micro-blocks A_{11} and A_{12} are

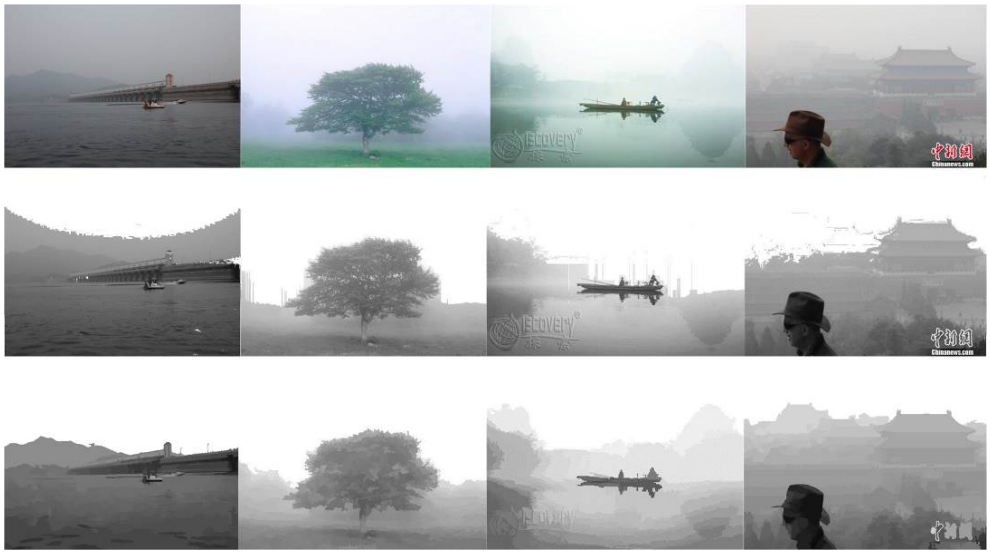

FIGURE 4. Comparison of segmented sky regions (white pixels), the first row shows the input hazed images, the second row shows the segmented sky regions by method in [7], the third row shows the segmented sky regions by the proposed method, from left to right: *wharf*, *tree*, *boat*, and *man_in_haze*.

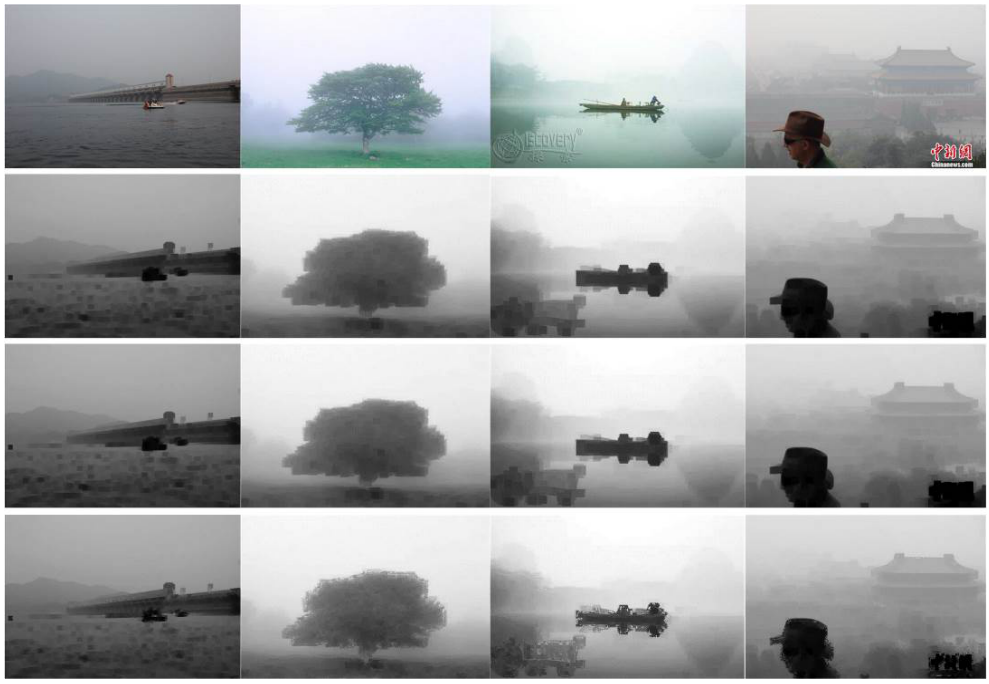

FIGURE 5. Comparison dark channel of my method and the methods in [6] and [7], the first row shows the input hazed images, the second row shows the dark channel calculated by method in [6], the third row shows the dark channel calculated by method in [7], the fourth row shows the dark channel calculated by the proposed method. Note that only the dark channel of non-sky regions are useful in the proposed method, from left to right: *wharf*, *tree*, *boat*, and *man_in_haze*.

selected as the feature pixels. After that, the corresponding two segmented areas (denoted as S_p and S_q) in which the two feature pixels locates are selected. Finally, all the areas which have similar luminance with S_p and S_q and connected with each other are selected to merge the sky region. From Fig. 4, it can be observed that the proposed method can extract sky regions accurately.

B. EDGE PRESERVING DARK CHANNEL OF INPUT HAZED IMAGE

Based on the dark channel prior assumption, the dark channel becomes better for a larger patch size because the probability that a patch contains a dark pixel is increased. But, at the same time, the medium transmission in a large patch may not be constant, e.g. a patch containing depth edges. Thus, in the

FIGURE 6. Estimated medium transmission of different methods, the first row shows the input hazed image, the second row shows the estimated medium transmission of the method in [6], the third row shows the estimated medium transmission of the method in [7], the fourth row shows the estimated medium transmission of the proposed method, from left to right: *wharf*, *tree*, *boat*, and *man_in_haze*.

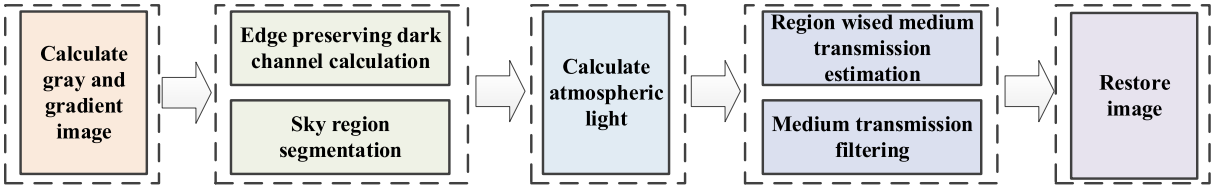

FIGURE 7. Block diagram of the proposed method.

proposed method, in non-edge region pixels, the patch size is set as a large value (15×15), while in edge region pixels, the patch size is set as a small value (3×3).

First, edges of the input hazed image $\mathbf{I}$ are detected, then the dark channel is generated by (14),

$$\mathbf{I}^{\mathbf{dark}}(\mathbf{x}) = \begin{cases} \min\limits_{\mathbf{y}\in\Omega_3(\mathbf{x})}\left[\min\limits_{c\in\{r,g,b\}}\mathbf{I}^c(\mathbf{y})\right] & \text{for edge region} \\ \min\limits_{\mathbf{y}\in\Omega_{15}(\mathbf{x})}\left[\min\limits_{c\in\{r,g,b\}}\mathbf{I}^c(\mathbf{y})\right] & \text{for non-edge region,} \end{cases} \tag{14}$$

where Ω_3 represents the patch with size of 3×3, and Ω_{15} represents the patch with size of 15×15. The results of the proposed dark channel are shown in Fig. 5. Note that only the dark channel of non-sky regions are useful for the following processing.

C. GLOBAL ATMOSPHERIC LIGHT

The atmospheric light usually corresponds to the thickest haze area [6], e.g. sky region, etc. Therefore, when there exist sky regions, the largest intensity of sky region is regarded as the atmospheric light. When there are no sky regions in the input image, the positions (denoted as $\mathbf{\Theta}$) of the brightest 10% pixels in the dark channel $\mathbf{I}^{\mathbf{dark}}(\mathbf{x})$ are first collected. Then, the largest intensity of the pixel at $\mathbf{\Theta}$ in the input hazed image $\mathbf{I}$ are regarded as the global atmospheric light.

D. REGION-WISED MEDIUM TRANSMISSION

For non-sky regions, the medium transmission can be calculated by (7) directly based on the dark channel prior. For sky regions, from (5), it can be derived that the medium transmission can be written as

$$\tilde{\mathbf{t}}_{sky}(\mathbf{x}) = \frac{1 - \min\limits_{\mathbf{y}\in\mathbf{\Omega}(\mathbf{x})}\left(\min\limits_{c\in\{r,g,b\}}\left(\mathbf{I}^c(\mathbf{y})./\mathbf{A}^c\right)\right)}{1 - \min\limits_{\mathbf{y}\in\mathbf{\Omega}(\mathbf{x})}\left(\min\limits_{c\in\{r,g,b\}}\left(\mathbf{J}^c(\mathbf{y})./\mathbf{A}^c\right)\right)}. \tag{15}$$

Usually, red (r) component is the minimum in the sky regions of a haze free image $\mathbf{J}$ [15]. Therefore,

$$\min_{\mathbf{y}\in\mathbf{\Omega}(\mathbf{x})}\left(\min_{c\in\{r,g,b\}}\left(\mathbf{J}^c_{sky}(\mathbf{y})./\mathbf{A}^c\right)\right) \approx \mathbf{J}^r_{\mathbf{\Omega}(\mathbf{x})}, \tag{16}$$

where $\mathbf{J}^r_{\mathbf{\Omega}(\mathbf{x})}$ is the r component of a patch $\mathbf{\Omega}(\mathbf{x})$ in the haze-free image $\mathbf{J}$. Thus, in order to calculate the medium

FIGURE 8. Hazed images used in the experiments.

FIGURE 9. Comparison of dehazed images, the first row shows the input hazed image, the second row shows the dehazed images of the method in [6], the third row shows the dehazed images of the method in [7], the fourth row shows the dehazed images of the proposed method, from left to right: *wharf, tree, boat, and man_in_haze.*

transmission of sky *regions*, $\mathbf{J}^r_{\Omega(\mathbf{x})}$ must be estimated. In this paper, it can be assumed that there exist a relationship between $\mathbf{J}^r_{\Omega(\mathbf{x})}$ and $\mathbf{I}^r_{\Omega(\mathbf{x})}$ for sky regions, i.e.,

$$\mathbf{J}^r_{\Omega(\mathbf{x})} = \eta \mathbf{I}^r_{\Omega(\mathbf{x})}, \tag{17}$$

which means that the r component of the patch $\Omega(\mathbf{x})$ in sky regions of the haze free image $\mathbf{J}$ come from an intensity attenuation (with a multiplicative coefficient $0 < \eta < 1$, the larger the haze is, the smaller η is) of $\mathbf{I}^r_{\Omega(\mathbf{x})}$. Since the pixel values of sky regions are consistent, the parameter η can be regarded as constant for all patches of sky regions.

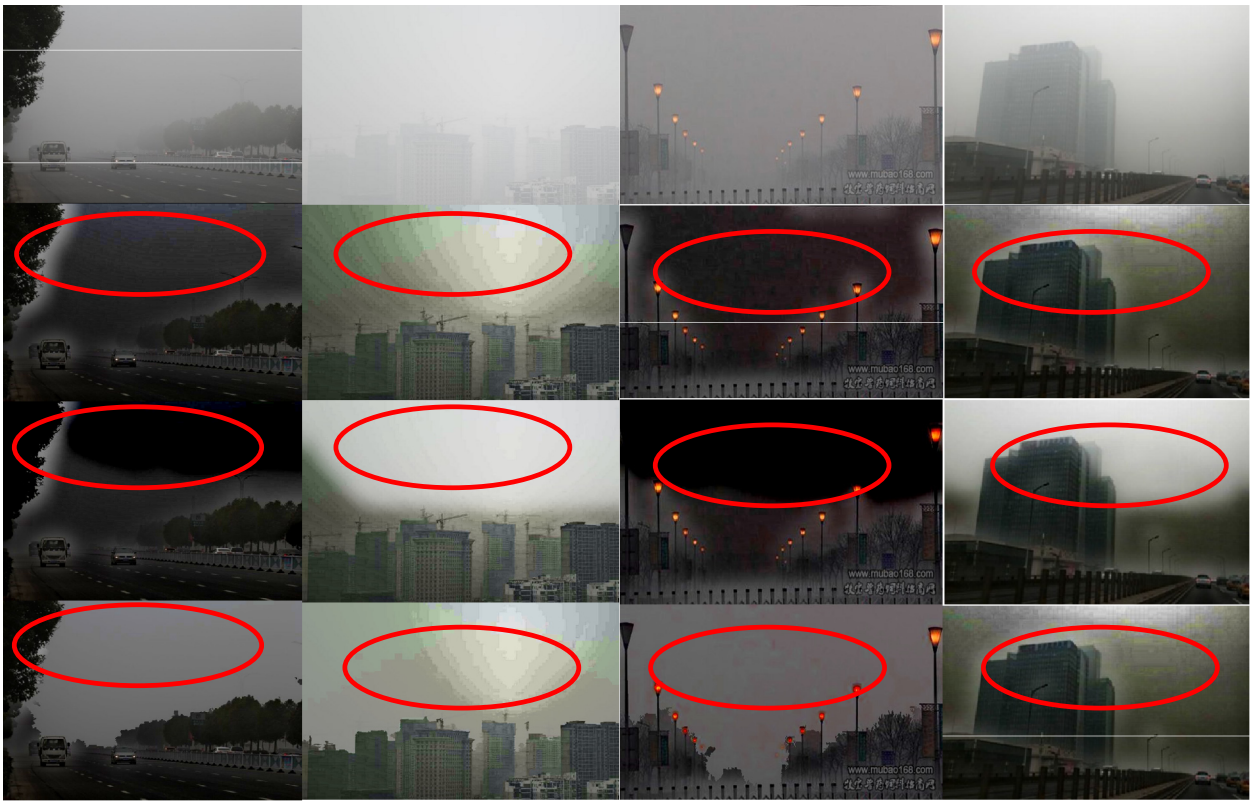

FIGURE 10. Comparison of dehazed images, the first row shows the input hazed image, the second row shows the dehazed images of the method in [6], the third row shows the dehazed images of the method in [7], the fourth row shows the dehazed images of the proposed method, from left to right: *road*, *city*, *streetlight*, and *building*.

Accordingly, $\tilde{\mathbf{t}}_{sky}(\mathbf{x})$ can be derived as,

$$\begin{aligned}\tilde{\mathbf{t}}(\mathbf{x})_{Sky} &= \frac{1-\min\limits_{\mathbf{y}\in\Omega(\mathbf{x})}\left(\min\limits_{c\in\{r,g,b\}}\left(\mathbf{I}^c(\mathbf{y})./\mathbf{A}^c\right)\right)}{1-\min\limits_{\mathbf{y}\in\Omega(\mathbf{x})}\left(\min\limits_{c\in\{r,g,b\}}\left(\mathbf{J}^c(\mathbf{y})./\mathbf{A}^c\right)\right)} \\ &= \frac{\mathbf{A}^c-\min\limits_{\mathbf{y}\in\Omega(\mathbf{x})}\left(\min\limits_{c\in\{r,g,b\}}\left(\mathbf{I}^c(\mathbf{y})\right)\right)}{\mathbf{A}^c-\min\limits_{\mathbf{y}\in\Omega(\mathbf{x})}\left(\min\limits_{c\in\{r,g,b\}}\left(\mathbf{J}^c(\mathbf{y})\right)\right)} \\ &\approx \frac{\mathbf{A}^c-\min\limits_{\mathbf{y}\in\Omega(\mathbf{x})}\left(\min\limits_{c\in\{r,g,b\}}\left(\mathbf{I}^c(\mathbf{y})\right)\right)}{\mathbf{A}^c-\mathbf{J}^r_{\Omega(\mathbf{x})}} \\ &= \frac{\mathbf{A}^c-\min\limits_{\mathbf{y}\in\Omega(\mathbf{x})}\left(\min\limits_{c\in\{r,g,b\}}\left(\mathbf{I}^c(\mathbf{y})\right)\right)}{\mathbf{A}^c-\eta\mathbf{I}^r_{\Omega(\mathbf{x})}}. \end{aligned} \tag{18}$$

Consequently, the medium transmission of the whole image can be calculated by

$$\tilde{\mathbf{t}}(\mathbf{x}) = \begin{cases} \dfrac{\mathbf{A}^c-\min\limits_{\mathbf{y}\in\Omega(\mathbf{x})}\left(\min\limits_{c\in\{r,g,b\}}\left(\mathbf{I}^c(\mathbf{y})\right)\right)}{\mathbf{A}^c-\eta\mathbf{I}^r_{\Omega(\mathbf{x})}} & \mathbf{x}\in \text{sky region} \\ 1-\omega\min\limits_{y\in\Omega(x)}\left(\min\limits_{c\in\{r,g,b\}}\dfrac{\mathbf{I}^c(y)}{\mathbf{A}^c}\right) & \mathbf{x}\notin \text{sky region}. \end{cases} \tag{19}$$

In addition, the medium transmission is filtered by guided filter [10]. In the filtering procedure, the patch size is set as 60×60 for non-edge pixel positions; while for edge pixel positions, the patch size is set as 12×12. Fig. 6 shows the final medium transmission of the proposed method. It can be observed that edge information is preserved better than other methods.

E. RECOVERING THE HAZY IMAGE

After obtaining the medium transmission $\tilde{\mathbf{t}}(\mathbf{x})$ and the atmospheric light (of different color component) $\mathbf{A}^c$, the haze free image can be estimated by using (9) directly. The block diagram of the proposed method is shown in Fig. 7.

IV. EXPERIMENTAL RESULTS

In order to verify the performance of the proposed method, the performance of the proposed method was compared with that of the method in [6] and the method in [7]. The configuration of the test platform is Windows 7 system with 2.0GHz CPU (Intel Core2 T6400) and 4GB memory. In the experiments, the parameter ω and η in (19) are set as 0.95 and 0.9 empirically, respectively. Eight hazed images, named as *wharf*, *tree*, *boat*, and *man_in_haze*, *road*, *city*, *streetlight,* and *building*, as shown in Fig. 8, are used to test the performance of the proposed method. Experimental results are shown in Fig. 9 and Fig. 10, from which it can be observed that the performance of the proposed method is

TABLE 1. Complexity comparison.

Image Name and Resolution	Computing Time(s)		
	Method in [6]	Method in [7]	Proposed Method
Wharf (809×537)	20.71	37.57	20.72
Tree (500×375)	5.17	6.54	5.42
Boat (500×300)	3.04	3.63	3.24
Man_in_haze(540x372)	5.28	7.59	5.37
Road (690×459)	10.86	11.27	11.15
City (834×549)	22.75	23.02	23.42
Streetlight (500×285)	2.75	2.97	2.95
Building(350×214)	1.00	1.11	1.22

better than the other two methods, especially in sky regions. Compared with the method in [7], the edges are preserved more precisely by the proposed method; while compared with the method in [6], the color discrepancy of the proposed method is smaller.

Besides, the time consumption of the three methods are also compared, as shown in TABLE I. It can be observed that the time consumption of the proposed method is comparable with the other two methods.

V. CONCLUSION

Since dark channel prior is not reasonable in sky regions, a sky region segmentation based image dehazing method is proposed in this paper. Sky regions are first segmented by quad-tree splitting based feature pixels detection and mean shift algorithm. Then, a region wised medium transmission estimation method is proposed. After that, an edge preserving guided filter is proposed to refine the medium transmission. As a result, the hazed image is restored based on the region wised the medium transmission and the atmospheric scattering model. Experimental results show that the proposed method is effective. There are less noise and color distortion in the restored image, especially for sky regions.

ACKNOWLEDGMENT

The authors would like to thank the editors and anonymous reviewers for their valuable comments.

REFERENCES

[1] Y. Wang and C. Fan, "Single image defogging by multiscale depth fusion," *IEEE Trans. Image Process.*, vol. 23, no. 11, pp. 4826–4837, Nov. 2014.
[2] I. Yoon, S. Kim, D. Kim, M. H. Hayes, and J. Paik, "Adaptive defogging with color correction in the HSV color space for consumer surveillance system," *IEEE Trans. Consum. Electron.*, vol. 58, no. 1, pp. 111–116, Feb. 2012.
[3] Y. Xu, J. Wen, L. Fei, and Z. Zhang, "Review of video and image defogging algorithms and related studies on image restoration and enhancement," *IEEE Access*, vol. 4, pp. 165–188, Mar. 2016.
[4] R. T. Tan, "Visibility in bad weather from a single image," in *Proc. IEEE Conf. Comput. Vis. Pattern Recognit. (CVPR)*, Anchorage, AK, USA, Jun. 2008, pp. 1–8.
[5] Y. Y. Schechner, S. G. Narasimhan, and S. K. Nayar, "Polarization-based vision through haze," *Appl. Opt.*, vol. 42, no. 3, pp. 511–525, Jan. 2003.
[6] K. He, J. Sun, and X. Tang, "Single image haze removal using dark channel prior," *IEEE Trans. Pattern Anal. Mach. Intell.*, vol. 33, no. 12, pp. 2341–2353, Dec. 2011.
[7] Y. Zhu, J. Liu, and Y. Hao, "A single image dehazing algorithm using sky detection and segmentation," in *Proc. IEEE Int. Congr. Image Signal Process. (CISP)*, Dalian, China, Oct. 2014, pp. 248–252.
[8] K. B. Gibson, D. T. Vo, and T. Q. Nguyen, "An investigation of dehazing effects on image and video coding," *IEEE Trans. Image Process.*, vol. 21, no. 2, pp. 662–673, Feb. 2012.
[9] J. Wang and M. F. Cohen, "Image and video matting: A survey," *Found. Trends. Comput. Graph. Vis.*, vol. 3, no. 2, pp. 97–175, Jan. 2007.
[10] K. He, J. Sun, and X. Tang, "Guided image filtering," in *Proc. IEEE 11th Eur. Conf. Comput. Vis. (ECCV)*, Crete, Greece, Sep. 2010, pp. 1–14.
[11] J.-H. Kim, J.-Y. Sim, and C.-S. Kim, "Single image dehazing based on contrast enhancement," in *Proc. IEEE Int. Conf. Acoust., Speech Signal (ICASSP)*, Prague, Czech Republic, May 2011, pp. 1273–1276.
[12] A. Cantor, "Optics of the atmosphere–scattering by molecules and particles," *IEEE J. Quantum Electron.*, vol. 14, no. 9, pp. 698–699, Sep. 1978.
[13] C. Tomasi and R. Manduchi, "Bilateral filtering for gray and color images," in *Proc. IEEE 6th Int. Conf. Comput. Vis. (ICCV)*, Bombay, India, Jan. 1998, pp. 839–846.
[14] D. Comaniciu and P. Meer, "Mean shift: A robust approach toward feature space analysis," *IEEE Trans. Pattern Anal. Mach. Intell.*, vol. 24, no. 5, pp. 603–619, May 2002.
[15] B. R. Babaria, T. L. Alvarez, M. T. Bergen, and R. J. Servatius, "Transmission of light in a synthetic fog medium," in *Proc. IEEE 30th Annu. Northeast Conf. Bioeng.*, Springfield, MA, USA, Apr. 2004, pp. 23–24.

HUI YUAN (S'08–M'12) received the B.E. and Ph.D. degrees in telecommunication engineering from Xidian University, Xi'an, China, in 2006 and 2011, respectively. From 2013 to 2014, he was a Post-Doctoral Fellow with the Department of Computer Science, City University of Hong Kong, Hong Kong. He is currently an Associate Professor with the School of Information Science and Engineering, Shandong University, Jinan, China. His current research interests include image and video processing, video compression, and multimedia communications.

CHANGCHUN LIU received the B.E. degree in telecommunication engineering from the Harbin Institute of Technology, Harbin, China, in 2006, and the M.S. degree in telecommunication engineering from Shandong University, Jinan, China, in 2016. He is currently a Lieutenant Colonel with the Chinese People's Liberation Army, China. His research interests include image and video processing.

ZHIXIN GUO received the B.E. and M.S. degrees in telecommunication engineering from Shandong University, Jinan, China, in 2013 and 2016, respectively. He is currently pursuing the Ph.D. degree with the Department of Telecommunications and Information Processing, Ghent University. His research interest includes image processing and computer vision.

ZHENZHEN SUN received the B.E. degree in telecommunication engineering from Shandong University, Jinan, China, in 2015. She is currently pursuing the M.S. degree with the School of Information Science and Engineering, Shandong University. Her research interest includes image and video processing.